



# Modeling Type Ic Supernovae with TARDIS: Hidden Helium in SN 1994I?

Marc Williamson<sup>1</sup> , Wolfgang Kerzendorf<sup>2</sup> , and Maryam Modjaz<sup>1</sup>   
<sup>1</sup>New York University, USA  
<sup>2</sup>Michigan State University, USA

Received 2020 October 15; revised 2020 December 8; accepted 2020 December 8; published 2021 February 19

## Abstract

Supernovae (SNe) with photospheric spectra devoid of hydrogen and helium features are generally classified as SNe Ic. However, there is ongoing debate as to whether helium can be hidden in the ejecta of SNe Ic (that is, helium is present in the ejecta, but produces no obvious features in the spectra). We present the first application of the fast, 1D radiative transfer code TARDIS to an SN Ic, and we investigate the question of how much helium can be hidden in the outer layers of the SN Ic ejecta. We generate TARDIS models for the nearby, well-observed, and extensively modeled SN Ic 1994I, and we perform a code comparison to a different, well-established Monte Carlo based radiation transfer code. The code comparison shows that TARDIS produces consistent synthetic spectra for identical ejecta models of SN 1994I. In addition, we perform a systematic experiment of adding outer He shells of varying masses to our SN 1994I models. We find that an outer He shell of only  $0.05M_{\odot}$  produces strong optical and near-infrared (NIR) He spectral features for SN 1994I which are not present in observations, thus indicating that the SN 1994I ejecta is almost fully He deficient compared to the He masses of typical He-rich SN progenitors. Finally we show that the He I  $\lambda 20851$  line pseudo-equivalent width of our modeled spectra for SN 1994I could be used to infer the outer He shell mass which suggests that NIR spectral follow-up of SNe Ic will be critical for addressing the hidden helium question for a statistical sample of SNe Ic.

*Unified Astronomy Thesaurus concepts:* Type Ic supernovae (1730); Core-collapse supernovae (304); Radiative transfer (1335); Astronomy data modeling (1859)

## 1. Introduction

Stripped-Envelope (SE) supernovae (SNe) are the core-collapse explosions of massive ( $>8M_{\odot}$ ) stars that have lost part or all of their outermost hydrogen and helium layers (Clocchiatti et al. 1997). In particular, SNe with photospheric spectra lacking hydrogen and helium features are classified as type Ic (SNe Ic, Filippenko et al. 1993; Modjaz et al. 2019). There are many potential underlying causes for the lack of both hydrogen and helium features in SNe Ic spectra. Stripping due to binary interaction (Podsiadlowski et al. 1992; Yoon 2015), line-driven winds for massive single progenitors (Crowther 2007; Smartt 2009), and homogeneous chemical evolution due to rotation (only for H, Maeder 1987; Langer 2012) are all possible mechanisms for removing the outer layers of SN Ic progenitors (for more review of SESNe progenitor scenarios see Smartt 2009; Yoon 2015).

In the last decade, the question of hidden He has arisen (i.e., He present in the SN ejecta without producing observable spectral absorption features). Complex radiative transfer simulations like CMFGEN (Hillier & Miller 1998) show that it is possible to hide up to the entire outer He layer (Dessart et al. 2012) if there is low mixing of  $^{56}\text{Ni}$ . In this case, optical He I lines are not present because they require non-thermal excitation by fast electrons which are produced through interactions with  $\gamma$ -rays from  $^{56}\text{Ni}$  and  $^{56}\text{Co}$  decay (Lucy 1991). However, there is also evidence for particular SNe Ic like SN 1994I where radiative transfer simulations show that optical He I lines do appear when an outer He layer of mass as low as  $\approx 0.10M_{\odot}$  is present (Hachinger et al. 2012, henceforth referred to as H12). Understanding how much He can be hidden in SNe Ic ejecta is crucial for understanding the SN Ic progenitor scenarios. Specifically, constraining the hidden helium content of SNe Ic ejecta will put constraints on the degree of progenitor

helium stripping required to produce observed SNe Ic. For binary system models (e.g. Woosley et al. 2020), the helium stripping is primarily achieved through mass transfer to the companion, and for massive single star scenarios the helium loss results from line-driven winds (Yoon 2017). Multiple theoretical studies have been published that discuss hidden helium focusing on different progenitor and explosion parameters like binary progenitor system parameters (Dessart et al. 2015) and the degree of  $^{56}\text{Ni}$  mixing (Dessart et al. 2012). However, there are very few modeling efforts in the literature dedicated to observed SNe Ic (Swartz et al. 1993; Iwamoto et al. 1994, 2000; Mazzali et al. 2000; Hachinger et al. 2012) and none perform a systematic investigation to constrain the possible amount of hidden helium. There is a clear need for such hidden helium focused modeling efforts for observed SNe Ic in order to understand the diversity of the SN Ic class.

SN 1994I is one of the best observed SNe Ic (Filippenko et al. 1995; Clocchiatti et al. 1996) since it occurred in the nearby galaxy M51. Recent analysis of the light curve (Drout et al. 2011; Bianco et al. 2014) and spectra (Modjaz et al. 2016; Williamson et al. 2019) has shown that SN 1994I may actually be relatively atypical compared to other SNe Ic. However, SN 1994I is an excellent choice for modeling due to the large number of modeling attempts in the literature (Baron et al. 1996; Sauer et al. 2006; Hachinger et al. 2012; Parrent et al. 2016) and high quality observational data (Filippenko et al. 1995; Clocchiatti et al. 1996). Despite the wealth of papers in the literature modeling SN 1994I, there has not been a systematic investigation to constrain the presence or amount of hidden He. Baron et al. (1996) model SN 1994I using PHOENIX, but their models are relatively insensitive to He abundance, so the He mass cannot be inferred. Sauer et al. (2006) use the Monte Carlo (MC) radiative transfer approach (Abbott & Lucy 1985; Lucy & Abbott 1993; Mazzali & Lucy 1993; Lucy 1999, 2002, 2003; Mazzali 2000), but their

simulations do not include the treatment of the important non-thermal fast electrons, which are known to affect the excitation state of He (Lucy 1991). More recently, H12 computed models of SN 1994I which included a treatment of the important non-thermal processes. H12 compute a model sequence between SN 1994I and the SN IIb 2008ax (e.g., Pastorello et al. 2008) by altering the density profile and H and He envelope masses, but their work lacks a systematic exploration of how much He can be contained in the SN 1994I ejecta. There is a clear need for such a systematic investigation into the possible presence and amount of He in the SN 1994I ejecta using a fast radiation transport code capable of treating the non-thermal processes.

In this paper, we perform a systematic set of spectral synthesis simulations using the open-source radiation transport code TARDIS (Kerzendorf & Sim 2014), which includes a treatment for non-thermal processes affecting He (Boyle et al. 2017), in order to place a strong upper limit on the amount of hidden He that can exist in the ejecta for SN 1994I. SN 1994I is a good candidate for understanding the hidden He question because there are relatively strong constraints on its progenitor scenario due to hydrodynamical modeling that simultaneously fit the monochromatic light curves (Iwamoto et al. 1994). Iwamoto et al. (1994) rule out the single Wolf-Rayet star progenitor scenario due to the fast decline of the SN 1994I light curve relative to other SNe Ic (Bianco et al. 2014). Further modeling by Van Dyk et al. (2016) narrows down the three binary system progenitor scenarios presented by Iwamoto et al. (1994) to SN 1994I resulting from the explosion of a low-mass C+O star with a low or intermediate mass main sequence binary companion. Both low (Iwamoto et al. 1994) and high (Sauer et al. 2006) degrees of  $^{56}\text{Ni}$  mixing have been proposed for the SN 1994I ejecta, but for the purposes of establishing an upper limit to the amount of hidden He, we adopt the low mixing CO21 model presented by Iwamoto et al. (1994) since increased mixing will produce stronger lines in the spectra, for the same He mass. Therefore, a low  $^{56}\text{Ni}$  mixing model is the most conservative choice for testing the maximum amount He that can be hidden in the SN 1994I ejecta.

As we will show with our TARDIS models of SN 1994I, distinct He I absorption features appear in the optical and near-infrared (NIR) spectra with an outer He shell of mass  $0.05M_{\odot}$ . In addition, we will show that not only is the He I 20851 line sensitive to the existence of trace amounts of He, but also how its pseudo-equivalent width (pEW) increases with increasing He outer shell mass.

In Section 2 we discuss the fast, 1D, time independent, open-source<sup>3</sup> radiation transfer code TARDIS used for our simulations. We present the methodology of our code comparison to a similar Monte Carlo based radiation transport code (H12) and the methodology for our detailed hidden He investigation. The results of our code comparison and hidden He investigation are presented in Section 3, and we conclude in Section 4.

## 2. Methods

In Section 2.1 we present details of the code TARDIS, the radiative transfer code used for the simulations in this work. We discuss specific parameter choices for our code comparison with H12 in Section 2.2, and we present our method for investigating the presence of hidden helium in SN 1994I models in Section 2.3.

### 2.1. TARDIS

TARDIS is an MC radiative transfer code based on the approach presented in Abbott & Lucy (1985), Lucy & Abbott (1993), Mazzali & Lucy (1993), Lucy (1999, 2002, 2003). For a given SN ejecta model, the user must provide the abundance and density structure as input, and TARDIS self-consistently solves for the ionization and excitation state of the plasma by propagating photon packets through the ejecta. TARDIS assumes homologous expansion, which is a reasonable assumption for the spectra we are modeling, since the ejecta stratification structure is mostly fixed by 5 days post explosion for the more extended progenitor stars of type IIP SNe (Tsang et al. 2020). For SNe with more compact progenitors like SN 1994I, homology is valid even earlier (Röpke 2005; Röpke & Hillebrandt 2005). Moreover, in this work we only model spectra between 16 and 40 days post explosion. In this early photospheric phase of evolution, TARDIS approximates the supernova as an optically thick core emitting a blackbody continuum, surrounded by more transparent outer shells which are responsible for absorption features. MC photon packets are assumed to originate from a blackbody profile at a constant velocity in the ejecta model. Photon packets accrue optical depth as they propagate through the ejecta and probabilistically experience either electron scattering or atomic line transitions. For the simulations presented in this paper, we use the Kurucz atomic data set (i.e., line list) for calculating the bound-bound transitions (Kurucz & Bell 1995) with the H and He lines taken from the CHIANTI 7.1 (Dere et al. 1997; Landi et al. 2012) database. TARDIS supports a full macroatom implementation of atomic transitions (Lucy 2002) as well as a modified version of macroatom called downbranch, in addition to pure scattering. While above we describe the general features of TARDIS, we proceed below to give more detailed information on the two settings in which we run TARDIS for SN 1994I.

### 2.2. Code Comparison

This paper is the first application of TARDIS to SNe Ic, so we conduct a code comparison to the similarly designed MC radiative transfer code used by H12 to model SN 1994I. Other radiative transfer codes have been used to model SN 1994I, but algorithmic differences between these codes and TARDIS would greatly obfuscate the code comparison. In particular, the PHOENIX code used by Baron et al. (1996) is time dependent (unlike TARDIS) and the MC code used by Sauer et al. (2006) does not include a treatment for the non-thermal excitation of Helium (unlike TARDIS). The code comparison to H12 allows us to test the analytic approximation of Boyle et al. (2017) that TARDIS uses to incorporate the non-thermal effects on He from fast electrons against the full non-local thermodynamic equilibrium (NLTE) treatment used in H12. We have obtained the low He mass ( $\sim 0.01M_{\odot}$ ) models of SN 1994I used in H12 (see Hachinger et al. 2012 Figure 5) for the SN 1994I spectra at phases 16, 22, 30, and 40 days post explosion (private communication Hachinger). For the code comparison, we use the H12 input models to generate TARDIS synthetic spectra and compare the TARDIS results to their model spectra presented in H12. In this section, we describe the TARDIS settings chosen to facilitate an equal comparison to H12, and the most important parameter choices are recorded in Table 1. The TARDIS configuration and model files are publicly available.<sup>4</sup>

<sup>3</sup> <https://github.com/tardis-sn/tardis>

<sup>4</sup> <https://github.com/tardis-sn/tardis-setup>

**Table 1**  
TARDIS Parameter Settings for Code Comparison

TARDIS Parameter	Setting
Ionization	nebular
Excitation	dilute-lte
Radiative Rate	dilute-blackbody
Line Interaction	downbranch
Number of Iterations	50
Number of Packets	$1.0 \times 10^5$
Helium Treatment	recomb-nlte

We run TARDIS using the `nebular` ionization mode and the `dilute-lte` excitation mode. This is a first order departure from a standard Saha–Boltzmann LTE treatment that accounts for dilution of the radiation field. Although TARDIS supports a full macroatom implementation of atomic transitions during bound–bound processes, we use `downbranch` mode for consistency with H12. The `dilute-blackbody` mode for radiative rate enforces that TARDIS calculates radiative rates in the same way as H12. One minor difference between TARDIS and the code used in H12 involves the treatment of energy deposition due to gamma-rays. Fast Compton electrons are produced due to gamma-rays from the  $^{56}\text{Ni}$  decay, and it has been shown that these non-thermal electrons have an effect on the ionization and excitation state of He (Lucy 1991). H12 use a light curve modeling code to simulate the creation and transport of gamma-rays and incorporate this information into their NLTE treatment. While TARDIS does not explicitly simulate gamma-rays, it supports the `recomb-nlte` He treatment (Boyle et al. 2017), which is an approximation for helium based on the simulations in H12 that show the He I ground state population is negligible due to non-thermal effects. The `recomb-nlte` mode treats the He I excited states as being in dilute LTE with the He II ground state, and calculates the He II excited states and He III ground state relative to the He II ground state.

We use the same density, abundance, and radiative temperature structure as H12. By forcing TARDIS to use the  $T_{\text{rad}}$  profile from H12, we are using TARDIS as an opacity calculator. The density profile is the result of the CO21 hydrodynamical simulation of a low-mass C+O stellar core explosion (Iwamoto et al. 1994). We adopt the CO21 model in order to facilitate an equal comparison with H12, which used the same model. However we note that there are many more recent stellar evolution models of stripped stars that may give rise to SESNe (Yoon 2017; Dessart et al. 2020; Laplace et al. 2020; Woosley et al. 2020).

### 2.3. Hidden Helium Investigation

Despite the large number of high quality observed spectra (Filippenko et al. 1995; Clocchiatti et al. 1996) and multiple synthetic models for SN 1994I (Baron et al. 1996; Sauer et al. 2006; Hachinger et al. 2012) in the literature, there has not been a systematic modeling investigation to determine the amount of helium that could be hidden in the SN 1994I ejecta. Constraining the helium content of SN 1994I and other SNe Ic will inform stellar evolution simulations of the progenitors of these explosions. Most massive stars are formed in binaries (Sana et al. 2012), and binary systems in particular are most likely responsible for the stripping necessary to produce SNe Ic (Dessart et al. 2011, 2020; Smith et al. 2011; Langer 2012; Schneider et al. 2020; Woosley et al. 2020). Hidden He can affect parameters of

the binary system like companion mass and type of mass transfer required to strip the right amount of He from the host (Dewi & Pols 2003). In addition, given recent advances in the understanding of Wolf–Rayet star mass-loss rates, it is possible that low-mass single He stars could be the progenitors for a fraction of SNe Ic (Yoon 2017). In this case, hidden He would affect our understanding of the degree of mass loss required to produce an explosion like SN 1994I.

In this section, we describe the systematic process used in this work to determine an upper limit on the mass of the outer He shell for SN 1994I. We use the same TARDIS settings as described in Section 2.2 to facilitate comparison of our upper limit He mass to the maximum total He mass range of  $0.06\text{--}0.14M_{\odot}$  resulting from the H12 model sequence. While the H12 model sequence involved modifying the density profile to have a more extended envelope, we obtain He limits within the CO21 model of SN 1994I. For each epoch of SN 1994I (we use the same observed data as in H12), we modify the abundance structure of the H12 models by replacing the outermost shells with a pure He shell. We perform the He shell replacement in such a way as to conserve the ejecta mass and note that the modification to the abundance structure from the H12 models is relatively minor. We repeat this modification for various masses of the outer He shell and each time generate synthetic spectra using TARDIS. We determine an upper limit on the outer He shell mass by comparing the TARDIS synthetic spectra to the observed SN 1994I spectra, specifically focusing on the He absorption wavelength regions. The upper He mass limit is chosen such that synthesized TARDIS spectra from models with outer He shell masses larger than that mass show noticeable He features that are not present in the observed spectra of SN 1994I.

## 3. Results

### 3.1. Results of Code Comparison

In order to thoroughly test TARDIS against the code from H12, we compare both the converged radiative temperature profiles ( $T_{\text{rad}}$ ), as well as the outputted synthetic spectra. For the  $T_{\text{rad}}$  comparison, we use the same ejecta models from H12 and allow TARDIS to self-consistently solve for a converged plasma state of the SN ejecta. This allows us to test the TARDIS internal plasma state calculations. The synthetic spectra comparison is also run using the same ejecta models from H12, but we also force TARDIS to use the converged  $T_{\text{rad}}$  and dilution factor ( $w$ ) profiles from H12 in order to focus the comparison on the implementation details of MC photon packet propagation.

Figure 1 shows the converged TARDIS radiative temperature profiles (main panel) and the fractional difference between the TARDIS and H12 temperature profile (lower panel). The radiative temperatures in each shell are the effective temperature of the radiation field exposed to that shell, where the initial blackbody energy distribution emanating from the inner boundary is modified by atomic interactions. At later times, the inner boundary velocity recedes, exposing hotter material closer to the center of the ejecta. We note that  $T_{\text{rad}}$  is not the same as the temperature of the photosphere. For Figure 1 we allow TARDIS to self-consistently solve for the radiative temperature of the ejecta shells instead of using the  $T_{\text{rad}}$  profile obtained from the authors of H12. The fractional difference between the TARDIS and H12 converged  $T_{\text{rad}}$  profiles is on the order of 10%, with even better agreement for the early

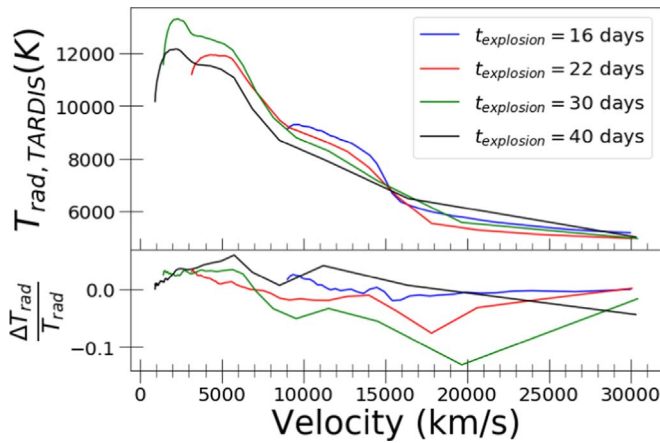


**Figure 1.** Comparison of the radiative temperature profiles from TARDIS and H12 as a function of ejecta velocity. Ejecta shells at higher velocities correspond to larger radii (due to homologous expansion) and encompass in total more mass. We note that  $T_{\text{rad}}$  is not the same as the temperature of the photosphere. The main panel shows the TARDIS  $T_{\text{rad}}$  profiles for each of the SN 1994I epochs considered in this paper. The lower panel shows the fractional difference  $(T_{\text{rad,TARDIS}} - T_{\text{rad,Hachinger}}) / T_{\text{rad,TARDIS}}$ . The TARDIS converged  $T_{\text{rad}}$  profile is in strong agreement with that of H12.

time (16 and 22 days) synthetic spectra. At later times when the inner boundary approximation to the photosphere is less appropriate, the codes may perform slightly differently due to minor implementation differences, but the fractional difference even for the 30 and 40 days spectra is still relatively small. Thus we find good general agreement between the TARDIS and H12  $T_{\text{rad}}$  profile calculations.

While the  $T_{\text{rad}}$  profile comparison showed general consistency in the radiation field and plasma calculations, we require another comparison to test the MC photon packet propagation between TARDIS and the MC code from H12. For this test we use the H12 input models ( $\sim 0.01M_{\odot}$  He) and compare the outputted synthetic spectra from both codes which are comprised of MC photon packets that have propagated through the SN ejecta and escaped. We force TARDIS to use the  $T_{\text{rad}}$  and  $w$  profiles from H12 in order to focus the comparison on the opacity calculations of each code. We also use the comparison of the synthetic spectra to check for consistency in the He I regions ( $\lambda 5876, 6678, 7065, 10831$ ) in order to validate the NLTE approximation used by TARDIS. Figure 2 shows the TARDIS synthetic spectra (blue) compared to the H12 synthetic spectra (red) at four epochs. The observed spectra (gray) are provided for reference. There is strong agreement between the codes for the 16 and 22 days synthetic spectra. In particular, the optical He I regions and the He I 10831 regions are generally consistent between the two synthetic spectra, validating the TARDIS approximation for non-thermal He excitation (Boyle et al. 2017). Noticeable differences between the synthetic spectra emerge in the later epochs of 30 and 40 days. The locations and widths of the synthetic spectral features generally match, but there are flux offsets, particularly in the Ca H & K and NIR triplet regions. The smaller flux offsets in the late time synthetic spectra are most likely due to minor differences in atomic data and/or algorithmic implementation exacerbated by the breakdown of the inner boundary approximation to the photosphere for late times. A detailed analysis of the TARDIS photon packets shows that the larger differences in the Ca H & K and NIR triplet regions is most likely due to fluorescence, but such detailed information for the individual MC photon packets is not

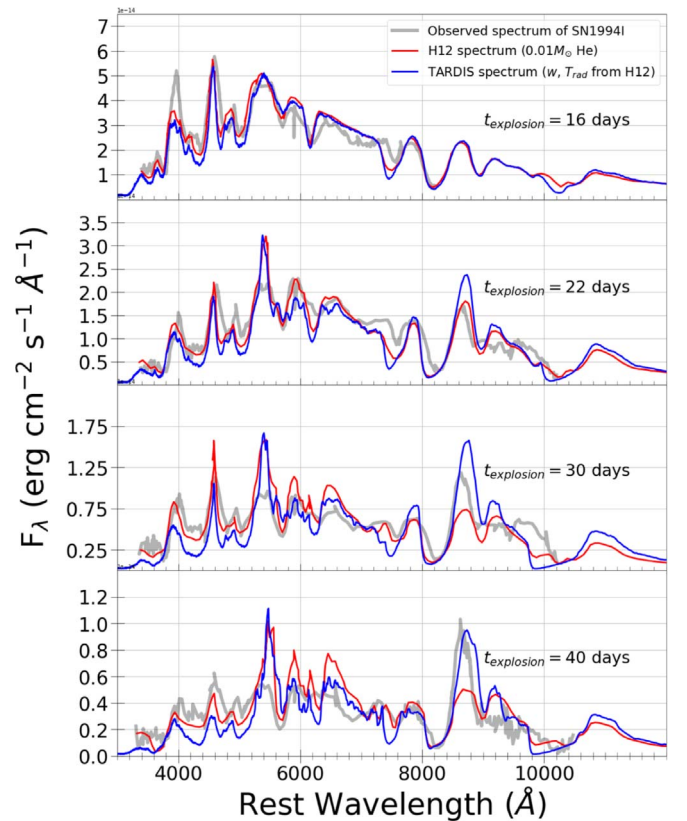


**Figure 2.** Direct comparison of the TARDIS synthetic spectra (blue) to the H12 synthetic spectra (red) for SN 1994I. Observed spectra for SN 1994I are provided for reference (Filippenko et al. 1995; Clocchiatti et al. 1996). TARDIS uses the abundance structure,  $T_{\text{rad}}$  profile, and dilution factor,  $w$ , profile from H12 and the settings from Table 1. See the text for detailed comparison of the models.

available for the H12 synthetic spectra. We note that the TARDIS model provides a better description of the observed Ca NIR triplet region (including what appears to be an emission-like feature) in SN 1994I.

### 3.2. Results of Hidden Helium Investigation

In order to put an upper limit on the amount of hidden He that could exist in the outer layer of the SN 1994I ejecta, we systematically insert progressively more massive ( $0.001M_{\odot}$ ,  $0.01M_{\odot}$ ,  $0.05M_{\odot}$ ,  $0.1M_{\odot}$ ) pure He shells into the models from H12 to test when noticeable He features appear in the synthetic spectra produced by TARDIS. As we will show, we find that for SN 1994I an outer He layer with mass as low as  $0.05M_{\odot}$  causes noticeable He features in the synthetic spectra that do not match observations. This is somewhat surprising given the low  $^{56}\text{Ni}$  mixing used by Iwamoto et al. (1994) which should make it easier to hide He in the outer layer of the SN 1994I ejecta. Figure 3 shows a detailed analysis of the He investigation for the  $t_{\text{explosion}} = 22$  days SN 1994I spectrum (we choose this spectrum because it is approximately 2 weeks after maximum light which is when He features are most apparent in observed SNe Ib. See Liu et al. 2016 for more details). We note that there are trace amounts of He in the inner layers totaling  $\sim 0.005M_{\odot}$  which were part of the original H12 model, but the contribution of this inner He to the synthetic spectrum is minimal compared to the He present in the outer layer.

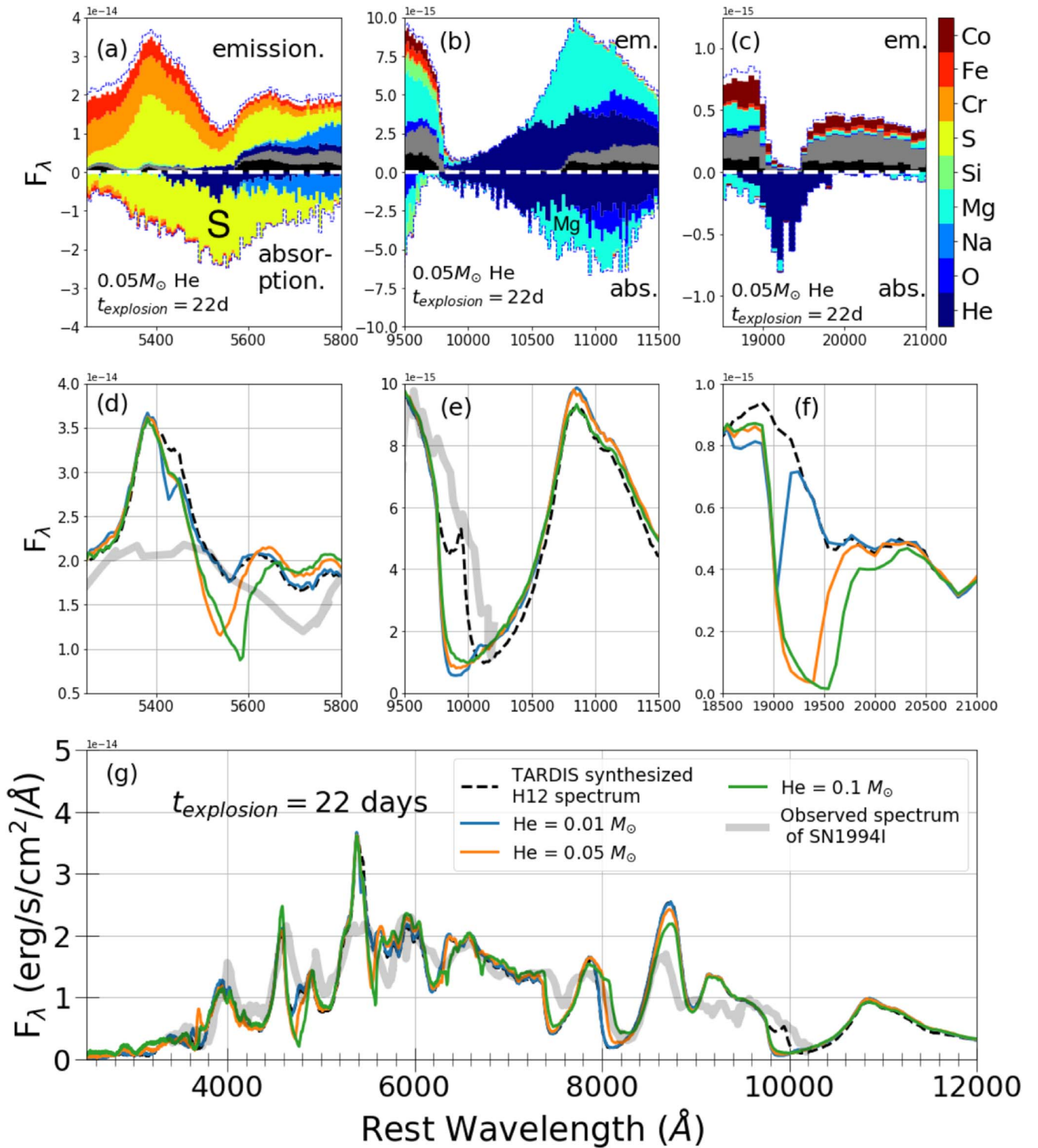


**Figure 3.** (a)–(c): Photon packet analysis of the SN 1994I  $t_{\text{explosion}} = 22$  days TARDIS synthetic spectrum with an outer He shell of  $0.05M_\odot$ . Colors above the dashed white line in the emission (em.) region indicate the element of the last interaction experienced by photons in a given wavelength bin. Black indicates contributions from photons that do not experience any interaction, and gray indicates photons where the only interaction is electron scattering. Colors below the dashed white line in the absorption (abs.) region indicate the last element responsible for removing a photon packet from a given wavelength bin via fluorescence. Dashed blue lines indicate the total emitted and absorbed spectrum, and we display colors for all elements with significant contributions to either emission or absorption in the relevant wavelength regions. (d)–(f): Zoom-ins of the He I 5876, He I 10831, and He I 20581 features from the synthetic spectra plotted in panel (g). (g): TARDIS synthetic spectra for SN 1994I using the H12 abundance model (black, dashed) compared to modified models to include outer He shells of masses  $0.01M_\odot$  (blue),  $0.05M_\odot$  (orange),  $0.10M_\odot$  (green). The observed spectrum is shown for reference (gray). Panel (c) shows that the He I 20581 line is uncontaminated by other elements, and panel (f) shows that the He I 20581 line is extremely sensitive to the outer He shell mass.

Since we are focusing on the question of hidden He, Figure 3 includes multiple panels zooming in on the He I 5876, 10831, and 20851 regions in the synthetic spectra. In order to securely

identify the synthetic spectral features with the elements in the ejecta model that produce them, we plot the last element responsible for interaction with an MC photon packet in the

topmost panels (a)–(c). These upper panels show the analysis of which elements contribute to the flux in each wavelength bin. Colors above the dashed white line (drawn at  $F_\lambda = 0$ ) indicate the element of the last interaction experienced by a photon packet in a given wavelength bin, thus indicating the last atom from which MC photon packets comprising the synthetic spectrum emerged. Colors below the white dashed line indicate the element last responsible for moving an MC photon packet out of a given wavelength bin via fluorescence, thus indicating the element last responsible for absorption. If a single element is responsible for the majority of the absorption, then it is reasonable to identify the corresponding synthetic spectral feature as being produced by that element. We note that the average number of interactions an MC photon packet experiences is  $\sim 1$ , so the last interaction is generally the only interaction (i.e., there are very few packets which experience multiple interactions). Henceforth we refer to the multi-colored plots shown in panels (a)–(c) of Figure 3 as spectral element decomposition plots (first introduced by Kromer et al. 2013, see their Figure 6). In order to determine the mass of the outer He layer for which noticeable He features appear in the synthetic spectra, the middle panels (d)–(f) of Figure 3 show zoom-ins of the He I 5876, 10831, and 20851 regions from each of the synthetic spectra shown in panel (g). We can see that an obvious He I feature that is not present in the observed SN 1994I spectrum appears in panel (d) in the TARDIS spectra with the low-mass  $0.05M_\odot$  He layer (we discuss the He I 10831 feature in more detail below).

In order to better understand the changes in the synthetic spectra shown in panels (d)–(f) as the mass of the inserted outer He layer increases, we produce the element spectral decomposition plots shown in panels (a)–(c) for each He outer layer mass (only the He mass =  $0.05M_\odot$  panels are shown in Figure 3). By examining the photon packets that escape the TARDIS simulations and contribute toward each synthetic spectrum we find that the depth of the trough at  $\sim 5550 \text{ \AA}$  increases as the outer He shell mass increases (see panel (d) of Figure 3) due to a larger number of photon packets being absorbed by He. However, it is clear from panel (a) that sulfur (yellow) is responsible for the majority of the absorption that produces the synthetic spectral feature at  $\sim 5550 \text{ \AA}$ . In particular, examining the TARDIS MC photon packets contributing to this feature reveals that the S II 5640 and S II 5606 lines dominate the absorption from He I 5876 and Na I D for this model of SN 1994I. While the blending of the Na I D and He I 5876 lines is well documented (Patat et al. 2001; Dessart et al. 2012), particularly with regard to SN 1994I (Clocchiatti et al. 1996; Sauer et al. 2006), sulfur is not discussed in the literature as a potential contaminant for the possible He I 5876 line in SNe Ic. This is somewhat surprising as it has been shown that S is produced through oxygen burning in shock-driven nucleosynthesis for core-collapse supernovae (Woosley & Weaver 1995; Woosley et al. 1995), and S is present in realistic models of SNe Ic (Dessart et al. 2015). In order for the S II 5640 and 5606 lines to contaminate the He I 5876 and Na I D lines (which are usually produced at high velocities in the SN ejecta), the S must be located at lower velocities in the ejecta. Figure 4 shows the velocity distributions of where in the SN 1994I ejecta the last bound–bound interactions occurred for He, Na, and S. As expected (since the S II 5604 and 5606 lines are bluer than He I 5876 and Na I D), we find that S line interactions occur much deeper in the ejecta than He and Na.

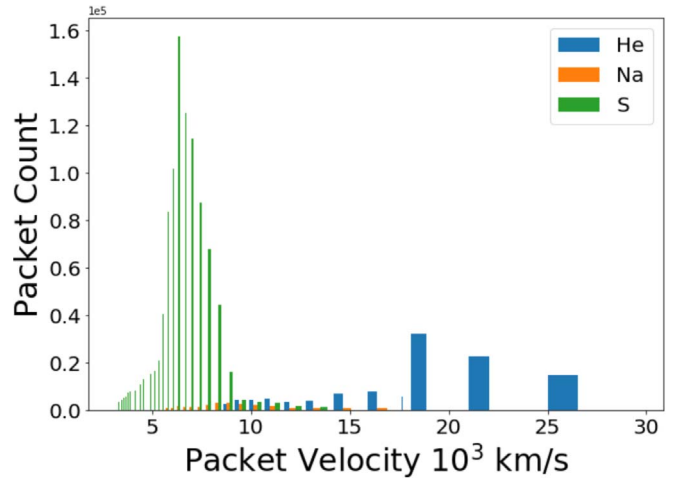


**Figure 4.** The velocity distributions of where the last interactions occurred for He (blue), Na (orange), and S (green) in the 22 days SN 1994I model with an outer He shell of mass  $0.05M_\odot$ . Low velocity (i.e., inner) He is negligible compared to the outer shell He. The distribution of S interactions is much deeper inside the ejecta than the high velocity He interactions.

This further complicates the He I 5876 line identification question in SNe Ic because the strengthening over time of the weak absorption feature seen in some observed spectra could be due to increased non-thermal excitation of He, blending with Na, or blending with lower velocity S as the photosphere recedes. Thus, we give supporting evidence to earlier suggestions that the SN Ib classification should not be based on just the He I 5876 line (Liu et al. 2016) given the contamination by other lines.

Just as we used the synthetic spectral element decomposition plots to analyze the potential He I 5876 feature in our TARDIS spectra, we apply a similar analysis to the potential NIR He I 10831 absorption feature. The identification of an absorption feature in the spectra of SN 1994I with He I 10831 has been thoroughly debated. There is some evidence that the inferred velocity of the potential He I 10831 feature is consistent with the velocities of extremely weak optical He I lines (Filippenko et al. 1995; Clocchiatti et al. 1996), but modelers have managed to reproduce the observed NIR absorption feature using Si I (Millard et al. 1999) and a mixture of He I and C I (Baron et al. 1996; Sauer et al. 2006). In this work we show that high velocity Mg can also be a contaminant of the He I 10831 feature, confirming a hypothesis from Filippenko et al. (1995) and work by Dessart et al. (2015). In particular, panel (b) of Figure 3 shows that the He I 10831 region is contaminated with Mg (cyan), confirming that it is not a good line for inferring the presence or mass of He in SN 1994I.

The reaction of the He I 10831 absorption feature in panel (e) of Figure 3 in response to increasing the mass of the inserted outer He layer appears counter-intuitive because the potential He I 10831 trough weakens as the outer He layer gains mass. However, a detailed analysis of the MC photon packets reveals that the number of packets absorbed by He actually increases with increasing outer He shell mass. The trough in the synthetic spectrum weakens instead of strengthening because by inserting the pure He shell, we are replacing some outer Mg which was contributing to the absorption comprising this feature. Thus the net effect is that the trough in the 1 micron region becomes slightly shallower with increasing He outer shell mass.

**Table 2**  
He I 20581 Pseudo-Equivalent Width

Phase <sup>a</sup> (days)	Injected He Mass ( $M_{\odot}$ )	pEW (Å)
16	0.001	N/A <sup>b</sup>
	0.01	64.03
	0.05	409.25
	0.10	609.52
22	0.001	145.53
	0.01	62.84
	0.05	482.64
	0.10	729.90
30	0.001	449.74
	0.01	446.13
	0.05	1182.32
	0.10	1187.99
40	0.001	555.53
	0.01	500.72
	0.05	453.35
	0.10	1492.34

**Notes.**

<sup>a</sup> Phase measured relative to date of explosion.

<sup>b</sup> There is no identifiable trough in the synthetic spectrum.

Finally, we apply the synthetic spectral element decomposition analysis shown in panel (c) of Figure 3 for day 22 of SN 1994I with a  $0.05M_{\odot}$  outer He shell to each of the TARDIS simulations shown in panel (f). The He I 20581 line is considered the most unambiguous indicator of He due to the lack of other nearby lines to act as contaminants (Dessart et al. 2015). Our TARDIS simulations for SN 1994I confirm that the He I 20581 region is uncontaminated, as shown in panel (c) of Figure 3. The colors below the dashed white line show that He is the dominant contribution toward the  $2\mu\text{m}$  trough. Specifically, more than 97% of the absorption between 1.9 and  $1.95\mu\text{m}$  is due to He. There are no observed spectra of SN 1994I including this feature, but our TARDIS simulations predict that the He I 20581 feature can be used for inferring outer He shell mass for future observations of SNe Ic. Panel (f) of Figure 3 shows that the He I 20581 line consistently changes as outer He shell mass increases. In Table 2 we calculate the pEW of the He I 20581 absorption feature in our synthetic spectra using the method from Liu et al. (2016), and we show that there is a clear trend of pEW increasing with increasing outer He shell mass. This result demonstrates the importance of NIR spectroscopy for constraining the He abundance of SNe Ic. To our knowledge, this is the first time that modeling has indicated that the outer He shell mass could be inferred from observations of the He I 20581 feature for SN 1994I-like objects. We note that TARDIS (as well as the H12 code) is a one-dimensional code and therefore does not probe potential asymmetries in the SN 1994I ejecta. There are two possible approaches to understand the role that ejecta asymmetries play in the hidden He question for SNe Ic: either multi-dimensional simulations (e.g., the work on understanding spectral variance of SN-GRBs with respect to viewing angle relative to the jet; Barnes et al. 2018) or radiation transfer modeling of a statistical sample of SNe Ic is required. The work presented here on SN 1994I is the first step in a larger effort using tardis to model a large number of SNe Ic.

## 4. Summary

In this paper, we present the first application of TARDIS to a SN Ic, 1994I. We perform a thorough investigation to determine an upper bound of  $0.05M_{\odot}$  for the mass of an outer He shell where obvious optical and NIR He features appear in the spectra. This result indicates that SN 1994I is almost completely He deficient in comparison with typical He masses ( $0.5\text{--}1.0M_{\odot}$ , Dessart et al. 2015) of He-rich SNe progenitors, although no observed spectra cover the He I 20581 line, which would provide the most confident assessment of He abundance. We present evidence for the first time that low velocity S II lines can be major contributors to blending of the He I 5876 line in SNe Ic. Moreover, the strengthening of He I 5876 absorption due to non-thermal effects is degenerate with the strengthening of the S II lines due to the recession of the photosphere over time. Finally, we show that not only is the He I 20581 line uncontaminated by other elements, but that it can also be used to infer the outer He shell mass using the pEW of the absorption feature. This highlights the critical importance of obtaining NIR spectra of SNe Ic in order to address the hidden helium question for a statistical sample of SNe. Future work will involve dedicated TARDIS modeling of the recent SN Ic 2020oi where NIR spectra are available (Rho et al. 2020). The SN 2020oi modeling will use the recently developed TARDIS emulator (Kerzendorf et al. 2020) which will enable us to produce posterior distributions for the He abundance. In addition, we will work to extend the TARDIS modeling capabilities to include new types of explosive phenomena with similar radiative transfer needs like fast blue optical transients (Modjaz et al. 2019; Pritchard et al. 2020).

The authors are extremely grateful to Stephan Hachinger for discussions on the differences between the TARDIS synthetic spectra and his work. We are also grateful for Dr. Hachinger's willing collaboration in sending us the initial conditions used in his simulations. M.M. and the SNYU group are supported by the NSF CAREER award AST-1352405, by the NSF award AST-1413260 and by a Humboldt Faculty Fellowship. M.M. thanks the MPIA for their hospitality. The tardis collaboration is a sponsored NumFOCUS project and is grateful for their support. We thank the Google Summer of Code and ESA Summer of Code in Space programs for supporting student contributions to tardis.

## ORCID iDs

Marc Williamson  <https://orcid.org/0000-0003-2544-4516>

Wolfgang Kerzendorf  <https://orcid.org/0000-0002-0479-7235>

Maryam Modjaz  <https://orcid.org/0000-0001-7132-0333>

## References

- Abbott, D. C., & Lucy, L. B. 1985, *ApJ*, 288, 679
- Barnes, J., Duffell, P. C., Liu, Y., et al. 2018, *ApJ*, 860, 38
- Baron, E., Hauschildt, P. H., Branch, D., Kirshner, R. P., & Filippenko, A. V. 1996, *MNRAS*, 279, 799
- Bianco, F., Modjaz, M., Hicken, M., et al. 2014, *ApJS*, 213, 19
- Boyle, A., Sim, S. A., Hachinger, S., & Kerzendorf, W. 2017, *A&A*, 599, A46
- Clocchiatti, A., Wheeler, J., Phillips, M., et al. 1997, *ApJ*, 483, 675
- Clocchiatti, A., Wheeler, J. C., Brotherton, M. S., et al. 1996, *ApJ*, 462, 462
- Crowther, P. A. 2007, *ARA&A*, 45, 177
- Dere, K. P., Landi, E., Mason, H. E., Monsignori Fossi, B. C., & Young, P. R. 1997, *A&AS*, 125, 149
- Dessart, L., Hillier, D. J., Li, C., & Woosley, S. 2012, *MNRAS*, 424, 2139

- Dessart, L., Hillier, D. J., Livne, E., et al. 2011, *MNRAS*, **414**, 2985
- Dessart, L., Hillier, D. J., Woosley, S., et al. 2015, arXiv:1507.07783
- Dessart, L., Yoon, S.-C., Aguilera-Dena, D. R., & Langer, N. 2020, *A&A*, **642**, 106
- Dewi, J. D. M., & Pols, O. R. 2003, *MNRAS*, **344**, 629
- Drout, M. R., Soderberg, A. M., Gal-Yam, A., et al. 2011, *ApJ*, **741**, 97
- Filippenko, A. V., Barth, A. J., Matheson, T., et al. 1995, *ApJL*, **450**, L11
- Filippenko, A. V., Matheson, T., & Ho, L. C. 1993, *ApJL*, **415**, L103
- Hachinger, S., Mazzali, P. A., Taubenberger, S., et al. 2012, *MNRAS*, **422**, 70
- Hillier, D. J., & Miller, D. L. 1998, *ApJ*, **496**, 407
- Iwamoto, K., Nakamura, T., Nomoto, K., et al. 2000, *ApJ*, **534**, 660
- Iwamoto, K., Nomoto, K., Höflich, P., et al. 1994, *ApJL*, **437**, L115
- Kerzendorf, W. E., & Sim, S. A. 2014, *MNRAS*, **440**, 387
- Kerzendorf, W. E., Vogl, C., Buchner, J., et al. 2020, arXiv:2007.01868
- Kromer, M., Fink, M., Stanishev, V., et al. 2013, *MNRAS*, **429**, 2287
- Kurucz, R., & Bell, B. 1995, Atomic Line Data Kurucz CD-ROM No. 23 (Cambridge, MA.: Smithsonian Astrophysical Observatory)
- Landi, E., Del Zanna, G., Young, P. R., Dere, K. P., & Mason, H. E. 2012, *ApJ*, **744**, 99
- Langer, N. 2012, *ARA&A*, **50**, 107
- Laplace, E., Göteborg, Y., de Mink, S., Justham, S., & Farmer, R. 2020, *A&A*, **637**, A6
- Liu, Y.-Q., Modjaz, M., Bianco, F. B., & Graur, O. 2016, *ApJ*, **827**, 90
- Lucy, L. B. 1991, *ApJ*, **383**, 308
- Lucy, L. B. 1999, *A&A*, **345**, 211
- Lucy, L. B. 2002, *A&A*, **384**, 725
- Lucy, L. B. 2003, *A&A*, **403**, 261
- Lucy, L. B., & Abbott, D. C. 1993, *ApJ*, **405**, 738
- Maeder, A. 1987, *A&A*, **178**, 159
- Mazzali, P. A. 2000, *A&A*, **363**, 705
- Mazzali, P. A., Iwamoto, K., & Nomoto, K. 2000, *ApJ*, **545**, 407
- Mazzali, P. A., & Lucy, L. B. 1993, *A&A*, **279**, 447
- Millard, J., Branch, D., Baron, E., et al. 1999, *ApJ*, **527**, 746
- Modjaz, M., Gutiérrez, C. P., & Arcavi, I. 2019, *NatAs*, **3**, 717
- Modjaz, M., Liu, Y. Q., Bianco, F. B., & Graur, O. 2016, *ApJ*, **832**, 108
- Parrent, J. T., Milisavljevic, D., Soderberg, A. M., & Parthasarathy, M. 2016, *ApJ*, **820**, 75
- Pastorello, A., Kasliwal, M., Crockett, R., et al. 2008, *MNRAS*, **389**, 955
- Patat, F., Cappellaro, E., Danziger, J., et al. 2001, *ApJ*, **555**, 900
- Podsiadlowski, P., Joss, P. C., & Hsu, J. J. L. 1992, *ApJ*, **391**, 246
- Pritchard, T. A., Bensch, K., Modjaz, M., et al. 2020, arXiv:2008.04321
- Rho, J., Evans, A., Geballe, T. R., et al. 2020, arXiv:2010.00662
- Röpke, F., & Hillebrandt, W. 2005, *A&A*, **431**, 635
- Röpke, F. K. 2005, *A&A*, **432**, 969
- Sana, H., de Mink, S. E., de Koter, A., et al. 2012, *Sci*, **337**, 444
- Sauer, D. N., Mazzali, P. A., Deng, J., et al. 2006, *MNRAS*, **369**, 1939
- Schneider, F. R. N., Podsiadlowski, P., & Müller, B. 2020, *A&A*, **645**, 5
- Smartt, S. J. 2009, *ARA&A*, **47**, 63
- Smith, N., Li, W., Filippenko, A. V., & Chornock, R. 2011, *MNRAS*, **412**, 1522
- Swartz, D. A., Filippenko, A. V., Nomoto, K., & Wheeler, J. C. 1993, *ApJ*, **411**, 313
- Tsang, B. T. H., Goldberg, J. A., Bildsten, L., & Kasen, D. 2020, *ApJ*, **898**, 29
- Van Dyk, S. D., De Mink, S. E., & Zapartas, E. 2016, *ApJ*, **818**, 75
- Williamson, M., Modjaz, M., & Bianco, F. B. 2019, *ApJL*, **880**, L22
- Woosley, S., Sukhbold, T., & Kasen, D. 2020, arXiv:2009.06868
- Woosley, S., & Weaver, T. A. 1995, The Evolution and Explosion of Massive Stars II: Explosive Hydrodynamics and Nucleosynthesis, Lawrence Livermore National Lab., CA, Tech. Rep. UCRL-ID-122106
- Woosley, S. E., Langer, N., & Weaver, T. A. 1995, *ApJ*, **448**, 315
- Yoon, S.-C. 2015, *PASA*, **32**, e015
- Yoon, S.-C. 2017, *MNRAS*, **470**, 3970